ADVANCED MATERIALS

[15] A. Peigney, C. Laurent, E. Flahaut, A. Rousset, *Ceram. Int.* **2000**, *26*, 677.
[16] A. Peigney, C. Laurent, F. Dobigeon, A. Rousset, *J. Mater. Res.* **1997**, *12*, 613.
[17] G. Zhan, J. D. Kuntz, J. Wan, A. K. Mukherjee, *Nat. Mater.* **2003**, *2*, 38.
[18] G. Zhan, J. D. Kuntz, J. E. Garay, A. K. Mukherjee, *Appl. Phys. Lett.* **2003**, *83*, 1228.
[19] R. Riedel, G. Passing, H. Schonfelder, R. J. Brook, *Nature* **1992**, *355*, 714.
[20] E. Kroke, Y. L. Li, C. Konetschny, E. Lecomte, C. Fasel, R. Riedel, *Mater. Sci. Eng., R* **2000**, *26*, 97.
[21] L. An, W. Zhang, V. M. Bright, M. L. Dunn, R. Raj, in *Proc. of the 13th IEEE Ann. Int. Conf. on Micro Electro Mechanical Systems*, Miyazaki, Japan **2000**, p 619.
[22] L. Bharadwaj, Y. Fan, L. Zhang, D. Jiang, L. An, *J. Am. Ceram. Soc.* **2004**, *87*, 483.
[23] Y. Cai, S. R. Shah, A. Zimmermann, M. Weinmann, R. Rai, F. Aldinger, *Phys. Status Solidi A* **2002**, *193*, R13.
[24] Y. Li, E. Kroke, R. Riedel, C. Fasel, C. Gervais, F. Babonneau, *Appl. Organomet. Chem.* **2001**, *15*, 820.
[25] S. Rajagopalan, R. Vaidyanathan, *JOM* **2002**, *54*, 45.
[26] B. R. Lawn, *J. Am. Ceram. Soc.* **1998**, *81*, 1977.
[27] P. K. Mallick, *Fiber-Reinforced Composites: Materials, Manufacturing and Design*, Marcel Dekker Inc., New York **1993**, p. 130.
[28] E. W. Wong, P. E. Sheehan, C. M. Lieber, *Science* **1997**, *277*, 1971.
[29] P. Poncharal, Z. L. Wang, D. Ugarte, W. A. de Heer, *Science* **1999**, *283*, 1513.
[30] Z. Pan, S. Xie, L. Lu, B. Chang, L. Sun, W. Zhou, G. Wang, D. Zhang, *Appl. Phys. Lett.* **1999**, *74*, 3152.
[31] X. Gong, J. Liu, S. Baskaran, R. D. Voise, J. S. Young, *Chem. Mater.* **2000**, *12*, 1049.
[32] J. M. Schwark, *US Patent 5 032 649*, **1991**.
[33] J. M. Schwark, *US Patent 4 929 704*, **1991**.

High-Efficiency Soft-Contact-Laminated Polymer Light-Emitting Devices with Patterned Electrodes**

By *Tae-Woo Lee*,* *Jana Zaumseil*, *Seong Hyun Kim*, and *Julia W. P. Hsu*

Organic light-emitting diodes (OLEDs) are well-suited for a wide range of existing and future display applications, especially when they are combined with flexible active-matrix circuits that incorporate organic thin-film transistors (OTFTs). OLEDs[1,2] and OTFTs[3] often use metal electrodes deposited directly onto the organic active layers by thermal or electron-beam evaporation or by sputtering.[1–5] In certain cases, this deposition process produces organic/metal interfacial regions characterized by metal in-diffusion and chemical or morphological disruption of the organic region.[4,6,7] Interfaces of this type can adversely affect the device performance, especially for OLEDs, where they potentially introduce quenching centers that can reduce quantum efficiencies and long-term stability. To avoid these problems, inactive buffer layers can be placed between the active organic region and the metal.[4] Our recent work suggests that OLEDs formed by physical lamination of metal electrodes to organic electroluminescent (EL) layers have fewer interfacial quenching sites and better quantum efficiencies than those formed by metal evaporation in vacuum.[8] This soft-contact lamination (ScL) approach relies upon van der Waals' interactions when an EL layer is brought into contact with a thin metal electrode supported by a conformable, elastomeric substrate. Unlike conventional lamination techniques,[9,10] this method does not require applied pressure, heating, or adhesives to establish high-quality electrical contacts. Since this method is inherently compatible with the tools of soft lithography,[11–13] it can be used to produce devices with geometries (i.e., OLED emissive areas or OTFT channel lengths) deep into the submicrometer range.[8,14–17]

Here we describe high-efficiency patterned and unpatterned organic light-emitting devices with Au electrodes by use of ScL with polymer EL layers that are blended with organic salts. Ionic species in polymer light-emitting devices greatly enhance the light intensity and luminous efficiency.[18–21] Expanding on previous work,[18] in which organic ammonium salts were shown to improve the efficiency of multilayer polymer EL devices, we blended the salts directly into the EL polymers. The dipole layers formed by organic salts at the electrode/organic interfaces enhance charge injection and reduce the dependence of device performance on the work function of the electrodes. The resulting devices differ from light-emitting electrochemical cells (LECs)[21] in that the ions are not mobile in organic-salt blend devices, because of the absence of an ion-conducting medium such as poly(ethylene oxide) (PEO). For the work presented here, we use Au as an electrode since it does not form a surface oxide. We compare the luminous efficiency and stability of these devices to those produced in the usual way by thermal evaporation of Au.

Figure 1a schematically illustrates the ScL process. The devices consist of two parts: 1) an elastomeric element of polydimethylsiloxane (PDMS) (shown with a relief structure designed to generate patterned emission) coated with a thin metal film, and 2) a transparent substrate that supports an electrode and an EL organic film. When these two components are brought together, van der Waals' interactions pull them into intimate contact at room temperature without any applied pressure. The resulting contact is mechanically robust, and cannot be peeled apart without additional force. We use the established techniques of soft lithography to form the elastomeric elements. In particular, a pre-polymer of PDMS

[*] Dr. T.-W. Lee, J. Zaumseil, Dr. J. W. P. Hsu
Bell Laboratories, Lucent Technologies
600 Mountain Avenue, Murray Hill, NJ 07974 (USA)
E-mail: taew.lee@samsung.com
Dr. S. H. Kim
Electronics and Telecommunications Research Institute
161 Gajeong-dong, Yuseong-gu, Daejeon 305-350 (Korea)

[**] We thank Dr. Z. Bao, Prof. J. A. Rogers, and Prof. O. O. Park for technical assistance, material support, and helpful comments. We thank Dr. M.-G. Kim for the helpful discussion.

  DOI: 10.1002/adma.200400182

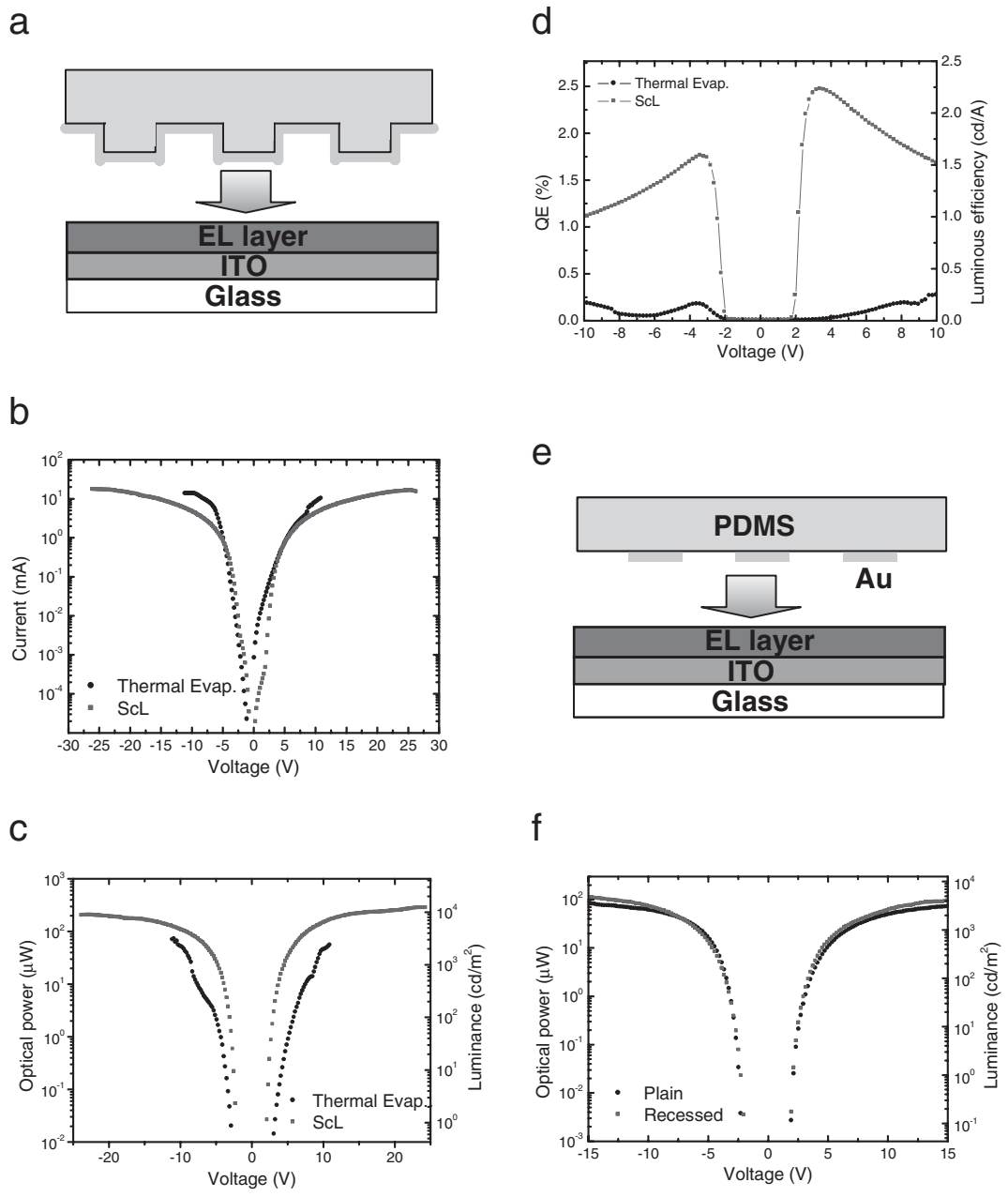

Figure 1. a) Schematic illustration of the ScL process for fabricating polymer EL devices by laminating a recessed Au/PDMS electrode with relief structure on the EL layer. The techniques of soft lithography can produce elements of the elastomer PDMS with fine features of surface relief (~2 μm depth). Blanket deposition of thin electrodes of Ti (1 nm)/Au (60 nm) forms an electrically continuous coating on the PDMS. A transparent substrate supports an EL layer on indium tin oxide. When these pieces are brought together, van der Waals' forces pull the electrodes into intimate contact with the EL layer at room temperature, without application of external pressure. The device characteristics of the ScL (■) and thermally evaporated (●) polymer EL devices based on a blend of MEH-PPV/TBABF$_4$ (in a ratio of 0.87:0.13 by weight), with an EL-layer thickness of 190 nm, are plotted as b) current–voltage, c) luminance–voltage, and d) device efficiency–voltage. The Au layer thickness was 60 nm. e) Schematic illustration of the ScL process for fabricating polymer EL devices by laminating patterned plain Au/Ti electrodes on PDMS. The electrodes can be patterned, by metal evaporation through a shadow mask, for example. f) The luminance–voltage characteristics of polymer EL devices fabricated by ScL with plain (●) and recessed (■) PDMS. Both the devices show similar behavior. The thickness of the evaporated Au layer in this case was 20 nm.

(Sylgard 184, Dow Corning) is cast and cured (60 °C for 3 h) on a Si wafer with or without a photoresist pattern on its surface. After peeling away from the master, the PDMS (~4 mm thick) is laminated to a glass slide and then exposed to an oxygen plasma for about 2 sec (Plasma-Therm reactive-ion etcher operating at 30 sccm, 30 mT, 100 V). Blanket deposition of Ti (1 nm, 0.3 nm s^{-1}) to promote adhesion, followed by Au (60 nm, in three sequential depositions of 20 nm at 1 nm s^{-1})

ADVANCED MATERIALS

produces the metal electrode. A transparent glass substrate supports a spin-cast blend EL layer on indium tin oxide (ITO). In this case, the blend consists of the EL polymer, poly(2-methoxy-5-(2′-ethylhexyloxy)-1,4-phenylenevinylene) (MEH-PPV) and the organic salt, tetrabutylammonium tetrafluoroborate ($TBABF_4$). Laminating these two elements together by hand in air completes the device. For patterned light output, a uniformly coated stamp with structured relief can be used (Fig. 1a), in which case only the contacting regions emit. Alternatively, patterns of metal electrodes can be formed on flat PDMS elements (Fig. 1e) by shadow-mask evaporation or soft lithography.

Figures 1b–d compare the characteristics of ScL and thermally evaporated devices. The current density versus voltage curve (Fig. 1b) shows an almost symmetric shape. Similar behavior is exhibited in the radiance versus voltage response (Fig. 1c), in spite of the difference in the work function (W) of Au ($W \sim 5.1$ eV) and ITO ($W \sim 4.7$ eV). Figure 1b shows that the current densities of the ScL and evaporated devices are similar in the range from –5 V to +8.8 V. The thermally evaporated device fails, however, at approximately +11 V in the forward and –11 V in the reverse direction. (The average breakdown voltage for 16 thermally evaporated devices in both directions was 10.6 ± 0.97 V.[22]) The current of the ScL device steadily increases beyond ±20 V, and eventually fails at ±26 V. (The average breakdown voltage for 21 ScL devices was 24.4 ± 3.8 V.) As shown in Figure 1c, the radiance versus voltage curve is also nearly symmetric. The EL intensity of the ScL device is, however, higher than that of the evaporated device. Figure 1d indicates that the highest luminous efficiency of the ScL device is ~2.25 cd A^{-1} (or ~2.5 % photons/electron, ph/el) (ITO-positive direction) and ~1.62 cd A^{-1} (or ~1.8 % ph/el) (Au-positive direction), at moderate voltages of +3.4 V and –3.4 V, respectively. (The average maximum efficiency for 12 ScL devices in the ITO+ direction was 2.12 ± 0.16 cd A^{-1}.) These values are nearly a factor of ten higher than those of the evaporated devices at these voltages. (The average maximum efficiency for eight evaporated devices in the ITO+ direction was 0.149 ± 0.077 cd A^{-1}.) We believe that the improved characteristics derive from favorable metal/organic interfacial properties in the ScL devices. Further study is required to understand the detailed chemical and morphological properties of the interfaces.

Patterned emission in ScL devices can be achieved in several ways, ranging from the use of structured PDMS elements, as illustrated in Figure 1a, to patterned metal electrodes on flat pieces of PDMS, as illustrated in Figure 1e. Figure 1f shows radiance versus voltage characteristics of ITO/MEH-PPV+$TBABF_4$ blend (190 nm)/Au(20 nm)/PDMS devices fabricated by both approaches; these devices (the flat-PDMS case used electrodes patterned by shadow mask evaporation) show the same characteristics. (The average device efficiency in the Au+ direction was 0.99 ± 0.17 cd A^{-1} for recessed PDMS and 1.00 ± 0.21 cd A^{-1} for flat PDMS, measured for eight devices for each type.) The flat PDMS approach has the advantage that the techniques of soft lithography (e.g., microcontact printing, phase-shift lithography) can be used to pattern the electrodes directly. Devices that use uniform coatings on structured PDMS elements have the advantage that the electrodes are effectively patterned at high resolution without exposing them to any form of processing (which could contaminate their surfaces and alter charge injection).

Figure 2a shows a schematic illustration of the polarization of organic salts near both electrodes during the operation of the polymer EL device of ITO/(EL blend layer with organic salts)/Au, where in this case the blend consists of MEH-PPV and $TBABF_4$. An applied electric field polarizes the salts and generates dipoles that improve the charge injection. Charge-carrier injection is believed to be enhanced similarly for devices that use dipole-adsorption layers, ionomers, single-ion conductors, and other ion-containing layers.[18–20,23–26] In those cases, dipoles near the electrodes create a drop in the energy barrier Φ at the interface for an applied field F, given by

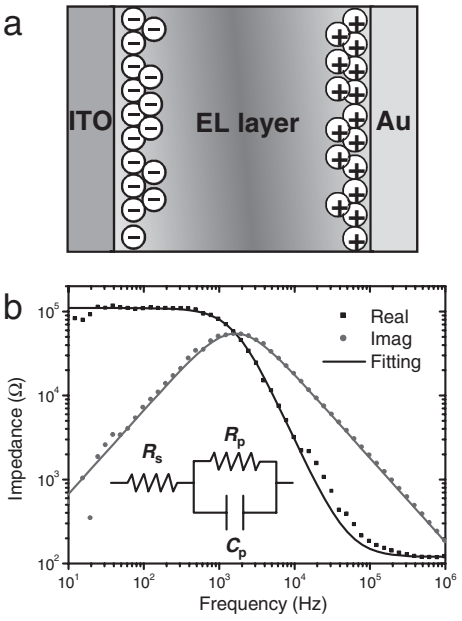

Figure 2. a) Schematic illustration of the role of organic salts ($TBABF_4$) in the polymer EL devices. Applied electric fields polarize the salts; the resulting dipoles near the electrodes improve charge injection. b) Impedance spectroscopy of the ScL device fabricated from the blend of MEH-PPV and $TBABF_4$, at 0 V DC bias. The inset shows the equivalent circuit, which can be described as a single parallel resistor R_p and capacitor C_p network with a series resistance R_s.

$$\Delta\Phi = F\,d = \sigma\,d/\varepsilon_o\,\varepsilon = N\,\mu/\varepsilon_o\,\varepsilon \quad (1)$$

where d is the distance between positive and negative partial charges, ε_o is the permittivity of vacuum, ε is the static dielectric constant, σ the surface charge density, N is the number of charges per unit surface, and μ is the dipole moment. Although this simple argument predicts that the barrier for charge injection decreases with the number of charges near

the electrodes, it is also important to note that the dipoles inside the active film may introduce scattering centers for charge transport, since their field will be oriented against the applied electric field.[24] One might therefore expect that there is a salt concentration that optimizes performance. For all of the devices described here, we did not attempt to identify the optimal concentration. Instead, we simply used an amount that yielded some significant improvement in the efficiency.

We performed alternating current (AC) impedance spectroscopy for ScL devices made of pure MEH-PPV and the blend of MEH-PPV and $TBABF_4$. Figure 2b shows impedance versus frequency data taken on a ScL device of the blend at 0 V direct current (DC) bias. The result is well fitted using the equivalent circuit shown in the inset of Figure 2b. The ScL device of pure MEH-PPV was also well fitted using the same circuit. The fitted parameters of pure MEH-PPV and the MEH-PPV/$TBABF_4$ blend devices formed by ScL are summarized in Table 1. Unlike in LEC devices,[27] the capacitance (C_p) does not show any noticeable change in response to the applied voltage in the salt-blend device, indicating ion dissociation does not occur and interior ions do not move to the electrodes. Therefore, the organic-solid-salt-doped MEH-PPV can form dipole moments in the device in the absence of an ion-conducting medium such as PEO. The series resistance (R_s) of organic-salt-doped MEH-PPV devices is lower than the pure MEH-PPV devices, favoring charge injection from the electrodes. As the bias voltage increases, the device resistance (R_p) becomes smaller as a result of charge-carrier injection.

Table 1. Parameters obtained by fitting the impedance data of the ScL devices to the equivalent circuit. DC voltages were applied to the Au electrode.

Material	Bias [V]	R_s [kΩ]	R_p [kΩ]	C_p [nF]
MEH-PPV	0	0.40	735	0.666
	1	0.40	590	0.667
	2	0.40	499	0.665
	4	0.40	359	0.660
	7	0.40	220	0.653
	15	0.40	72	0.655
MEH-PPV +$TBABF_4$	0	0.12	110	0.884
	3	0.12	48	0.905
	6	0.12	16	0.851
	9	0.12	14	0.875
	12	0.12	13	0.900

The EL device based on the blend of MEH-PPV with $TBABF_4$ tended to form dark spots during operation under ambient conditions. For this reason, we used commercially available polyfluorene derivatives supplied by Dow Chemical[28] to examine patterned emission and to quantify device stability. Figure 3 shows optical micrographs of patterned emission from an ScL EL device operating under an ITO-positive-bias field. This device uses a blend of a polyfluorene derivative with 17 wt.-% of $TBABF_4$ (100 nm). Figures 3a,b are reflection optical microscopy images of devices that use Au electrodes patterned on PDMS by microcontact printing of hexadecanethiol "inks", followed by wet etching and a short exposure to an oxygen plasma to remove the printed thiol. The devices, with Au electrode linewidths of 12 μm and 3 μm, appeared clean and free of cracking, as observed by optical and scanning electron microscopies. This device shows stable operation under ambient conditions; dark-spot growth was not observed even after 1–2 h of operation at voltages from 4 to 7 V. Thermally evaporated devices (with Au or Al) that use the same EL material show dark spots after operation for as little as a few seconds.

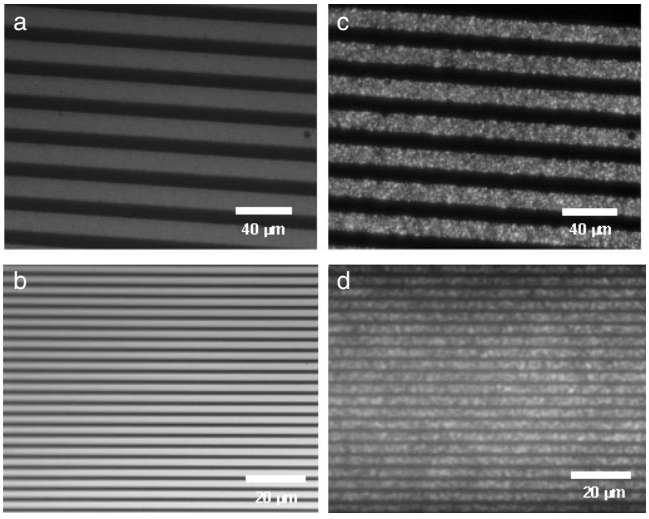

Figure 3. Optical microscopy of devices formed by ScL with patterned Au electrodes on PDMS, corresponding to the device type shown in Figure 1e. Reflection images of devices with a) 12 μm and b) 3 μm Au-patterned microcontact-printed lines. c,d) EL from (a) and (b), respectively. In all cases, the Au was 20 nm thick and the EL layer is composed of polyfluorene derivative blended with 17 wt.-% of $TBABF_4$ (100 nm thick layer).

To quantify these observations, we fabricated ScL and evaporated devices with EL layers of the polyfluorene derivative without the organic salts but with a poly(3,4-ethylenedioxythiophene):poly(styrene sulfonate) layer (PEDOT:PSS) between ITO and the emitting layer. In this case, a polyfluorene layer without salts was used to eliminate salt-related degradation pathways. The PEDOT:PSS layer between ITO and the EL layer reduces the effect of ITO on the device stability.[29] Figure 4 shows that operation of ScL and evaporated devices using these materials at current densities of 30 mA cm^{-2} (high enough to induce rapid aging of the devices) revealed similar short-term degradation (within 30 min). The ScL device, however, exhibited stable output after this initial stage, while the evaporated device continued to rapidly degrade. We believe that these differences might be due to interfacial differences that could also influence the device efficiencies.[30]

In summary, we demonstrated high-efficiency patterned polymer light-emitting devices formed by ScL and a blend of

ADVANCED MATERIALS

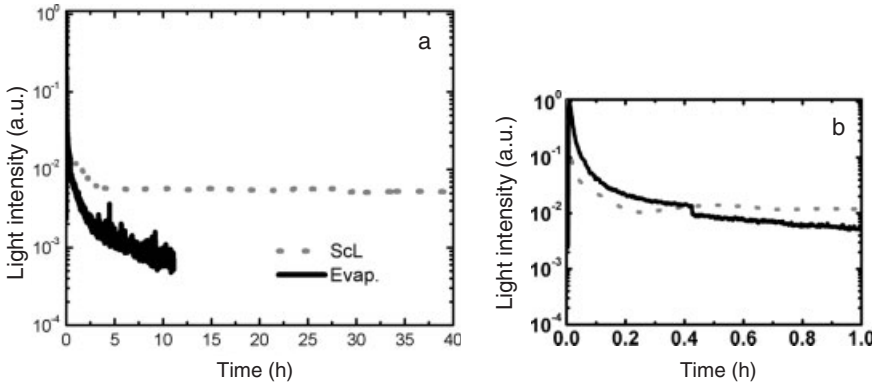

Figure 4. a) Aging tests of ITO/PEDOT:PSS/polyfluorene(100 nm)/Au (20 nm) devices formed by ScL and evaporation. The devices were operated at a high current density of 30 mA mm^{-2}. b) Luminescence decay within 1 h. The initial light intensities of the two devices were normalized to their maxima. The test was performed in a flowing-nitrogen-gas environment.

EL polymer with organic salts, achieved even with a high-work-function metal, Au. The blend of EL polymer with organic salts was employed as an emitting layer to improve the charge-injection efficiency at the EL layer/electrode interface according to the electrostatic Equation 1. Impedance spectroscopy showed that the organic solid salt forms dipole layers inside the film without dissociation under a DC electric field. Our study suggests that the ScL device can be greatly improved by modifying the EL layer without changing the work functions of the electrodes. Devices of this type show electrical and optical characteristics nearly independent of bias polarity. The ScL device showed higher efficiency than the thermally evaporated devices when the same EL and electrode materials were used. We also showed that it is possible to produce high-efficiency patterned EL devices that have micrometer-scale light-emitting areas by combining ScL with the established techniques of soft lithography. The ScL devices also showed better stability under electrical stress. These results suggest that ScL may represent a useful tool for studying OLED behavior, enabling devices that have well-controlled organic/electrode interfaces. In addition, we believe that the reversibility of the ScL contacts will be useful for studies of device degradation.

Experimental

Spin-casting forms a uniform film of the electroluminescent material (a mixture of poly(2-methoxy-5-(2′-ethylhexyloxy)-1,4-phenylenevinylene), MEH-PPV, or a polyfluorene derivative and tetrabutylammonium tetrafluoroborate, $TBABF_4$) on a thin layer (190 nm for MEH-PPV, 100 nm for the polyfluorene) of indium tin oxide (ITO; sheet resistance ~ 15 Ω □$^{-1}$) on a glass slide (0.4 mm thick). When the bottom (ITO/emitting layer) and top pieces (Au/polydimethylsiloxane, PDMS) are brought together, van der Waals' forces pull the electrodes into intimate contact with the electroluminescent (EL) layer at room temperature, without application of external pressure. Typically, this contact initiates on one side of the structure; a wetting front then progresses naturally across the sample until the entire surface is in contact. The vertical blanket deposition of Ti (adhesion promoter, 1 nm, 3 Å s^{-1})/Au (20–60 nm, 10 Å s^{-1}) over both the mold PDMS with relief structure and flat PDMS was performed by an electron-beam evaporator (Temescal BJD 1800) while rotating the samples with distance of 40.6 cm between the PDMS and the metal source during the evaporation. The metal-coated PDMS was used either to build devices immediately after evaporation, or after removal from brief storage in a dry-nitrogen environment. The thermally evaporated device was fabricated by evaporating the Au at a rate of 1 Å s^{-1} on the same materials described above using an Edward Auto 306 thermal evaporator with a distance of 29.2 cm between the samples and the metal source. An electrical poling to obtain the best performances from the EL devices was performed as described in the literature [31].

After microcontact printing, the Au/PDMS was exposed to oxygen plasma for 5–10 s, which was followed by soft-contact lamination in the same manner as described above. We followed the same microcontact-printing process as reported in the literature [11,12,14]. We observed the complete lamination over the entire surface through a microscope after laminating the top electrode over the electroluminescent materials on the ITO-glass substrate. We blended the MEH-PPV (molecular weight MW ~ 90 000 g mol^{-1}, H. W. Sands) with $TBABF_4$ (Aldrich) in a ratio of 0.865:0.135 by weight and with the polyfluorene derivative (Dow Green B, Dow Chemical) in a ratio of 0.83:0.17 by weight. For the aging study, we fabricated evaporated and laminated devices of ITO/poly(3,4-ethylenedioxythiophene):poly(styrene sulfonate) (PEDOT:PSS)/polyfluorene/Au structure. A 35 nm thick PEDOT:PSS (Bayer) layer was spin-cast on ITO and baked at 110 °C in a vacuum oven for 50 min. The impedances of the samples are measured by an impedance gain/phase analyzer (SI1260, Solatron) at 0.05 V alternating-current bias.

Received: February 9, 2004
Final version: June 15, 2004

[1] C. W. Tang, S. A. Van Slyke, *Appl. Phys. Lett.* **1987**, *51*, 913.
[2] R. H. Friend, R. W. Gymer, A. B. Holmes, J. H. Burroughes, R. N. Marks, C. Taliani, D. D. C. Bradley, D. A. Dos Santos, J.-L. Brédas, M. Lögdlund, W. R. Salaneck, *Nature* **1999**, *397*, 121.
[3] C. D. Dimitrakopoulos, D. J. Mascaro, *IBM J. Res. Dev.* **2001**, *45*, 11.
[4] L. S. Hung, L. S. Liao, C. S. Lee, S. T. Lee, *J. Appl. Phys.* **1999**, *86*, 4607.
[5] J. Xue, S. R. Forrest, *Appl. Phys. Lett.* **2001**, *79*, 3714.
[6] F. Faupel, R. Willecke, A. Thran, *Mater. Sci. Eng., R* **1998**, *22*, 1.
[7] J. Birgerson, M. Fahlman, P. Bröms, W. R. Salaneck, *Synth. Met.* **1996**, *80*, 125.
[8] T.-W. Lee, J. Zaumseil, Z. Bao, J. W. P. Hsu, J. A. Rogers, *Proc. Natl. Acad. Sci. U. S. A.* **2004**, *101*, 429.
[9] T.-F. Guo, S. Pyo, S.-C. Chang, Y. Yang, *Adv. Funct. Mater.* **2001**, *11*, 339.
[10] N. C. Greenham, R. H. Friend, D. D. C. Bradley, *Adv. Mater.* **1994**, *6*. 491.
[11] Y. Xia, G. M. Whitesides, *Angew. Chem. Int. Ed.* **1998**, *37*, 550.
[12] J. L. Wilbur, A. Kumar, H. A. Biebuyck, E. Kim, G. M. Whitesides, *Nanotechnology* **1996**, *7*, 452.
[13] H. Schmid, H. Wolf, R. Allenspach, H. Riel, S. Karg, B. Michel, E. Delamarche, *Adv. Funct. Mater.* **2003**, *13*, 145.
[14] Y.-L. Loo, T. Someya, K. W. Baldwind, Z. Bao, P. K. H. Ho, A. Dodabalapur, H. E. Katz, J. A. Rogers, *Proc. Natl. Acad. Sci. U. S. A.* **2002**, *99*, 10 252.

[15] Y.-L. Loo, R. L. Willett, K. W. Baldwin, J. A. Rogers, *Appl. Phys. Lett.* **2002**, *81*, 562.
[16] C. Kim, M. Shtein, S. R. Forrest, *Appl. Phys. Lett.* **2002**, *80*, 4051.
[17] Y. Koide, M. W. Such, R. Basu, G. Evmenenko, J. Cui, P. Dutta, M. C. Hersam, T. J. Marks, *Langmuir* **2003**, *19*, 86.
[18] T.-W. Lee, H.-C. Lee, O. O. Park, *Appl. Phys. Lett.* **2002**, *81*, 214.
[19] F. Huang, A. G. MacDiamid, *Appl. Phys. Lett.* **1998**, *76*, 2415.
[20] Y. Sakuratani, M. Asai, M. Tokita, S. Miyata, *Synth. Met.* **2001**, *123*, 207.
[21] Q. Pei, G. Yu, C. Zhang, Y. Yang, A. J. Heeger, *Science* **1995**, *269*, 1086.
[22] The error bar represents one standard deviation.
[23] F. Nüesch, E. W. Forsythe, Q. T. Le, Y. Gao, L. J. Rothberg, *J. Appl. Phys.* **2000**, *87*, 7973.
[24] S. H. Kim, K.-H. Choi, H.-M. Lee, D.-H. Hwang, L. M. Do, H. Y. Chu, T. Zyung, *J. Appl. Phys.* **2000**, *87*, 882.
[25] T.-W. Lee, O. O. Park, L.-M. Do., T. Zyung, T. Ahn, H.-K. Shim, *J. Appl. Phys.* **2001**, *90*, 2128.
[26] T.-W. Lee, O. O. Park, *Adv. Mater.* **2001**, *13*, 1274.
[27] Y. Li, J. Cao, G. Yu, Y. Cao, A. J. Heeger, *Chem. Phys. Lett.* **1998**, *287*, 83.
[28] M. T. Bernius, M. Inbasekaran, *Adv. Mater.* **2000**, *12*, 1737.
[29] A. Elschner, F. Bruder, H.-W. Heuer, F. Jonas, A. Karbach, S. Kirchmeyer, S. Thurm, R. Wehrmann, *Synth. Met.* **2000**, *111–112*, 139.
[30] A previous report (S. F. Lim, L. Ke, W. Wang., S. J. Chua, *Appl. Phys. Lett.* **2001**, *78*, 2116) states that the film pinholes in the evaporated device give rise to the growth of dark spots. However, physical lamination by soft, conformable electrodes has an advantage in that film pinholes will not make contact with the conformable electrodes. Although we did not observe the symptoms of pinholes from the current density at low voltages of our evaporated devices, pinholes could be a source for growth of dark spots in evaporated devices.
[31] T.-W. Lee, O. O. Park, *Appl. Phys. Lett.* **2000**, *77*, 3334.

High Efficiency Fine Particulate Filtration Using Carbon Nanotube Coatings**

By *Gunaranjan Viswanathan*, *David B. Kane*,* and *Peter J. Lipowicz*

The ultimate goal of carbon nanotube research is the fabrication of functional macroscopic structures that can fully utilize the individual nanotube properties. Although ordered nanotube assemblies[1,2] are required for making integrated devices, simpler macroscopic constructs that reflect the intrinsic random fiber morphology of the nanotubes offer potential applications such as media for aerosol filtration. Although gas-phase filtration properties of nanotube macrostructures have never been studied, there have been reports on nanotube pore structure[3,4] and gas permeability of nanotube membranes.[5] In this communication, we present the first investigation of the use of multiwalled carbon nanotubes (MWNTs) as highly efficient, airborne particulate filter media. Filter efficiencies in excess of 99 % were achieved from films of MWNTs deposited onto cellulose fiber filters. The MWNT-coated filters exhibited low pressure drops and better filter quality than cellulose filters even for very low MWNT coverages (0.07 mg cm^{-2}). The MWNT filter performance was comparable to the highest efficiency HEPA (high efficiency particulate air) filter standards.

Filtration of airborne particulate matter is essential in many instances, including air purifiers, respiratory protection equipment, and clean rooms. Fibrous filters are the most common type of filter media used for such applications, and are usually made from cellulose, glass, or polymer fibers. Fibrous aerosol filters do not work like sieves (that allow only particles smaller than the holes to pass through), rather, the mechanisms of interception of particles by the fiber surface, inertial impaction of a particle on a fiber, and Brownian diffusion of particles in the filter pores are mainly responsible for particle retention in the filter. These three mechanisms each dominate for different particle sizes. Fiber diameter is an important parameter that affects filter performance. Typically filters have fiber diameters on the order of 10 μm, therefore filters made from nanotubes with diameters in the range of 20–50 nm should display unique properties due to their small dimensions.

Figure 1 shows scanning electron microscopy (SEM) images of the MWNT-coated filter morphology. The top view (Figs.

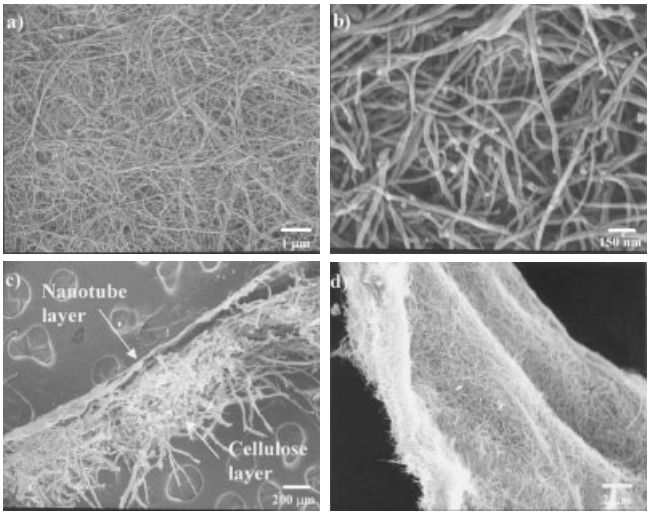

Figure 1. SEM images of MWNT-coated filters. a) Top view shows a fibrous filter morphology and b) high magnification image of (a). c) Cross-sectional view shows a continuous MWNT film (~ 1–2 μm thick, as seen in (d)) on top of the cellulose layer.

[*] Dr. D. B. Kane, G. Viswanathan,[+] Dr. P. J. Lipowicz
Philip Morris USA Research Center
4201 Commerce Road
Richmond VA 23234 (USA)
E-mail: david.b.kane@pmusa.com
[+] Present Address: Department of Chemical Engineering, Rensselaer Polytechnic Institute, Troy, NY 12180, USA.

[**] The authors thank Mark Zhuang for his help with the BET analysis. We also thank George Karles, Vicki Baliga, Randall Baren, and Prof. P. M. Ajayan (RPI) for valuable assistance and fruitful discussions relating to this work. We are grateful to NanoTechLabs Inc., for the MWNT samples.

DOI: 10.1002/adma.200400463